Journal of Power Sources 221 (2013) 366–371

Contents lists available at SciVerse ScienceDirect

Journal of Power Sources

journal homepage: www.elsevier.com/locate/jpowsour

Structures and electrochemical properties of $Li_{1.075}V_{0.925-x}M_xO_2$ (M = Cr or Fe, $0 \le x \le 0.025$) as new anode materials for secondary lithium batteries

Won-Tae Kim [a], Yeon Uk Jeong [a,*], Hyun Chul Choi [b], Yong Joong Lee [c], Young Jun Kim [d], Jun Ho Song [d]

[a] School of Materials Science and Engineering, Kyungpook National University, 80 Daehak-ro, Buk-gu, Daegu 702-701, South Korea
[b] Department of Chemistry, Chonnam National University, Gwangju 500-757, South Korea
[c] School of Mechanical Engineering, Kyungpook National University, Daegu 702-701, South Korea
[d] Advanced Batteries Research Center, Korea Electronics Technology Institute, Seongnam 463-816, South Korea

HIGHLIGHTS

- $Li_{1.075}V_{0.9}Fe_{0.025}O_2$ exhibits the first discharge capacity of 295 mAh g^{-1}.
- Cyclability was improved by the doping of iron in $Li_{1.075}V_{0.925-x}O_2$.
- $Li_{1.075}V_{0.9}Fe_{0.025}O_2$ exhibits an excellent rate capability.

ARTICLE INFO

Article history:
Received 7 May 2012
Received in revised form
11 July 2012
Accepted 31 July 2012
Available online 23 August 2012

Keywords:
Lithium-ion batteries
Anode materials
Lithium vanadium oxide
Chromium doping
Iron doping

ABSTRACT

$Li_{1.075}V_{0.925-x}M_xO_2$ (M = Cr or Fe, $0 \le x \le 0.025$) compounds are investigated as new anode materials for secondary lithium batteries. Previous research suggests $Li_{1+x}V_{1-x}O_2$ ($0.075 \le x \le 0.1$) samples exhibit the first discharge capacities of 240–250 mAh g^{-1} at 0.2 C-rate. Although the lithiation of $Li_{1+x}V_{1-x}O_2$ ($0.075 \le x \le 0.1$) offer high initial capacities, a major difficulty for the anode application lies in the cycle life. In an attempt to improve $Li_{1.075}V_{0.925}O_2$, doping with chromium and iron are systemically carried out to investigate its effect on the crystal structures, valence state of vanadium ions, electrical conductivities, mechanical strengths, and electrochemical properties. $Li_{1.075}V_{0.925-x}M_xO_2$ samples are successfully synthesized by solid-state reaction in a reducing atmosphere and the products give a single phase of the hexagonal layered structure with a space group of R-3m. Compared to $Li_{1.075}V_{0.925}O_2$, iron-doped materials give improved electrical conductivities and electrochemical properties. $Li_{1.075}V_{0.9}Fe_{0.025}O_2$ sample exhibits the highest discharge capacity, an excellent rate capability, and an improved cyclability due to the high strength of the individual particles.

1. Introduction

Various carbon-based materials were investigated as the anode materials for secondary lithium batteries. Mesocarbon microbead (MCMB) was commercialized in the early days, which had a high packing density and a reversible electrochemical behavior [1]. Thereafter, the synthetic graphite was replaced by the natural graphite which offered a higher energy density and lower cost. In an attempt to develop new anode materials for advanced applications, oxide-based materials such as $Li_4Ti_5O_{12}$ [2–6] and $Li_{1+x}V_{1-x}O_2$ [7–10] are recently investigated. Compared to $Li_4Ti_5O_{12}$, $Li_{1+x}V_{1-x}O_2$ anodes exhibit lower potentials and higher energy densities. Previous research suggests $Li_{1+x}V_{1-x}O_2$ ($0.075 \le x \le 0.1$) samples exhibit higher capacities than those of $Li_{1+x}V_{1-x}O_2$ ($0 \le x \le 0.05$) [9]. Electrochemical behaviors are strongly dependent on the compositions of the phases resulting from the significant differences in the local electronic structures [9]. Although the lithiation of $Li_{1+x}V_{1-x}O_2$ ($0.075 \le x \le 0.1$) to $Li_{1+x+y}V_{1-x}O_2$ ($0.075 \le x \le 0.1$) contributes to very high initial capacities in the low potential region (0.5–0.01 V vs. Li), a major difficulty for the anode application lies in the poor cycle life. Poor cycle life is related with the breakage of particles during the lithiation process. Recently, the intercalation mechanism for the lithiated $Li_{1+x}V_{1-x}O_2$ is proposed [10]. In this study, in an attempt to improve $Li_{1.075}V_{0.925}O_2$, doping with chromium and iron that have similar ionic radii is systemically carried out to investigate its effect on the crystal structures, valence state of vanadium ions, electrical conductivities, mechanical strengths, and electrochemical properties.

* Corresponding author. Tel.: +82 53 950 7586; fax: +82 53 950 5645.
E-mail address: jeong@knu.ac.kr (Y.U. Jeong).

0378-7753/$ – see front matter © 2012 Elsevier B.V. All rights reserved.
http://dx.doi.org/10.1016/j.jpowsour.2012.07.134

2. Experimental

$Li_{1.075}V_{0.925-x}M_xO_2$ (M = Cr or Fe) samples were prepared by solid-state reaction. Required amounts of Li_2CO_3, V_2O_5, Cr_2O_3, and Fe_2O_3 were mixed in a mortar for 1 h and pellets were prepared using mixed powders for heat treatment. In order to reduce V^{5+} to V^{3+}, pellets were heated in the mixed gas of 90% N_2 and 10% H_2 at 550 °C for 14 h, followed by heating at 1200 °C for 5 h to obtain the complete reaction products. X-ray powder diffraction (Cu Kα) and Rietveld refinement were carried out to characterize the crystal structure of the products. Lattice constants, distances and angles between ions were calculated from the X-ray diffraction data. Particle sizes and surface morphology of the prepared samples and cycled electrodes were evaluated by scanning electron microscopy (S.E.M.), Hitachi S-4200. The oxidation state of metal ions was investigated by X-ray photoelectron spectroscopy (XPS). The spectra were obtained with a VG multilab 2000 equipment (ThermoVG scientific) using non-monochromatized Mg Kα radiation (1253.6 eV). Core peaks were collected using a pass energy of 20 eV. No charge neutralization was used. The pressure in the analysis chamber was kept below 10^{-7} Pa. The binding energy scale was calibrated from the hydrocarbon contamination using the C 1s peak at 285.0 eV. In order to evaluate the electrical conductivities of the products by van der Pauw method, pellets with the size of 10×10 mm^2 and the thickness of 2 mm were prepared by sintering. Mechanical strengths of the individual particles were measured by compression tests using an ultra-micro hardness tester (Shimadzu MCT-211 series) with a loading rate of 35 mN s^{-1}.

The electrochemical properties were evaluated by using coin cells (2032-type). The slurries were prepared by mixing 80 wt.% $Li_{1.075}V_{0.925-x}M_xO_2$ (M = Cr or Fe) with 10 wt.% Super P carbon as a conducting additive, 10 wt.% polyvinylidene fluoride (PVDF) as a binder, and N-methyl pyrrolidone (NMP) as a solvent. Prepared slurries were coated onto the copper foil of 10 μm thickness followed by drying in an oven at 120 °C and cold pressing. For electrolytes, 1 M $LiPF_6$ was dissolved in the mixed solution of ethylene carbonate (EC) and ethyl methyl carbonate (EMC) with the ratio of 1:2. Lithium metal was used as the counter electrode and coin cells were assembled in an Ar-filled glove box. The charge/discharge tests were performed between 2.0 and 0.01 V with various C-rates, and the current value for 1 C-rate was fixed at 220 mAh g^{-1}. Cyclabilities of the cells were measured with the conditions of 0.2 C-rate charge and 0.5 C-rate discharge. Cyclic voltametry was carried out with a scan rate of 20 μV s^{-1}.

3. Results and discussion

The results of X-ray powder diffraction of $Li_{1.075}V_{0.925-x}Cr_xO_2$ ($0 \le x \le 0.1$) samples are shown in Fig. 1. $Li_{1.075}V_{0.925-x}Cr_xO_2$ ($0 \le x \le 0.075$) samples have a single phase of the hexagonal layered structure with a space group of R-3m [11]. Li_3CrO_4 impurities were found in $Li_{1.075}V_{0.925-x}Cr_xO_2$ ($x > 0.075$) samples. In the case of $Li_{1.075}V_{0.925-x}Fe_xO_2$ ($0 \le x \le 0.1$), as shown in Fig. 2, iron impurities are detected in the samples of $x > 0.025$. The solubility limits for chromium and iron in $Li_{1.075}V_{0.925-x}M_xO_2$ (M = Cr or Fe) are found at $x = 0.075$ and 0.025, respectively. Lattice parameters, specific position of oxygen (z_{oxygen}), distances, and angles between the ions in $Li_{1.075}V_{0.925-x}M_xO_2$ are summarized in Table 1. Lithium, metals (V, Cr, Fe, and excess Li) and oxygen ions occupied 3b site (0,0,0), 3a site (0,0,1/2) and 6c site (0,0,z), respectively. The lattice constants of a-axis are increased and those of c-axis are decreased with the increase in chromium or iron contents in $Li_{1.075}V_{0.925-x}M_xO_2$ (M = Cr or Fe).

While the bond distances of Li–O decrease with the increase in x, the bond distances of M–O increase with doping in

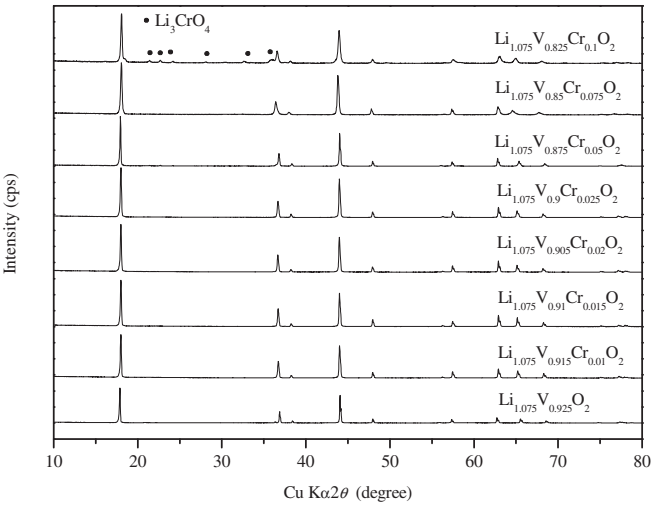

Fig. 1. X-ray powder diffraction patterns of $Li_{1.075}V_{0.925-x}Cr_xO_2$ ($0 \le x \le 0.1$).

$Li_{1.075}V_{0.925-x}M_xO_2$ (M = Cr or Fe). The angles of O_1–Li–O_2 and O_1–M–O_4 increase, but those of O_1–Li–O_4 and O_1–M–O_2 decrease with doping. Variations in the distances and angles between the ions and the difference in the ionic radii ($r_{V3+} = 0.64$ Å, $r_{Cr3+} = 0.615$ Å, $r_{Fe3+} = 0.645$ Å, $r_{Li+} = 0.76$ Å in a six-fold coordination environment, respectively) result in the change of MO_2-slab thickness and the inter-slab distance. As shown in Fig. 3, the thickness of MO_2-slab increase and the inter-slab distance decrease with the increase in x for $Li_{1.075}V_{0.925-x}M_xO_2$ (M = Cr or Fe). Various S.E.M. images of $Li_{1.075}V_{0.925-x}M_xO_2$ samples are shown in Fig. 4. $Li_{1.075}V_{0.925-x}Fe_xO_2$ samples have a larger average particle size compared to $Li_{1.075}V_{0.925-x}Cr_xO_2$ samples. Similar ionic radius of iron with vanadium might facilitate the particle growth upon heating.

To elucidate the valence state of Cr and Fe in the synthesized $Li_{1.075}V_{0.925-x}M_xO_2$ (M = Cr or Fe, $0 \le x \le 0.025$) compounds, XPS analysis are carried out and the result is shown in Fig. 5. The binding energies of an electron in Cr $2p_{3/2}$, Cr $2p_{1/2}$, Fe $2p_{3/2}$, and Fe $2p_{1/2}$ are determined at 573.9, 583.5, 711.1, and 724.7 eV, respectively. The observed values suggest that the valence states of Cr and Fe in the samples are mainly +3 states, which are consistent with the previous results [12,13]. Moreover, a noticeable shift of the

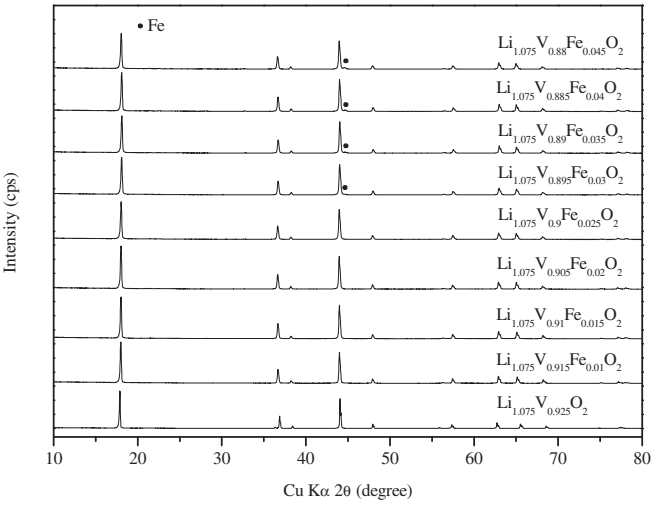

Fig. 2. X-ray powder diffraction patterns of $Li_{1.075}V_{0.925-x}Fe_xO_2$ ($0 \le x \le 0.045$).

Table 1
Lattice parameters, specific position of oxygen (z_{oxygen}), distances, and angles between the ions in $Li_{1.075}V_{0.925-x}M_xO_2$ samples.

Composition	a_{hex} (Å)	c_{hex} (Å)	z_{oxygen}	Distance (Å)		Angle (°)			
				Li–O	M–O	O_1–Li–O_2	O_1–Li–O_4	O_1–M–O_2	O_1–M–O_4
$Li_{1.075}V_{0.925}O_2$	2.848	14.718	0.2432	2.112	1.994	84.77	95.23	91.18	88.82
$Li_{1.075}V_{0.915}Cr_{0.010}O_2$	2.854	14.678	0.2439	2.106	2.000	85.28	94.72	91.02	88.98
$Li_{1.075}V_{0.910}Cr_{0.015}O_2$	2.853	14.690	0.2447	2.099	2.007	85.60	94.40	90.61	89.39
$Li_{1.075}V_{0.905}Cr_{0.020}O_2$	2.855	14.687	0.2452	2.096	2.011	85.84	94.16	90.40	89.60
$Li_{1.075}V_{0.900}Cr_{0.025}O_2$	2.857	14.669	0.2448	2.099	2.009	85.76	94.24	90.67	89.33
$Li_{1.075}V_{0.915}Fe_{0.010}O_2$	2.857	14.674	0.2439	2.108	2.001	85.30	94.70	91.11	88.89
$Li_{1.075}V_{0.910}Fe_{0.015}O_2$	2.859	14.668	0.2441	2.107	2.004	85.46	94.54	91.03	88.97
$Li_{1.075}V_{0.905}Fe_{0.020}O_2$	2.861	14.663	0.2445	2.104	2.007	85.68	94.32	90.88	89.12
$Li_{1.075}V_{0.900}Fe_{0.025}O_2$	2.862	14.660	0.2445	2.104	2.008	85.70	94.30	90.90	89.10

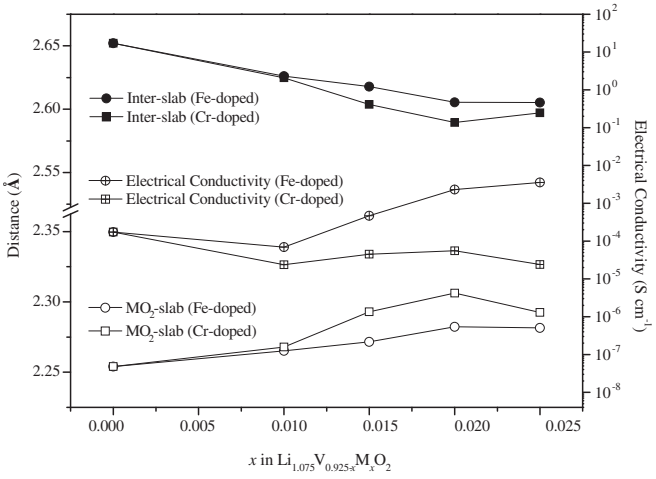

Fig. 3. Calculated MO_2-slab thickness, inter-slab distance by Rietveld refinement and electrical conductivities of $Li_{1.075}V_{0.925-x}M_xO_2$ ($0 \le x \le 0.025$).

maximum photoemission line of O 1s and V 2p is not observed with the increase in Cr and Fe contents. This indicates that the synthesized $Li_{1.075}V_{0.925-x}M_xO_2$ (M = Cr or Fe, $0 \le x \le 0.025$) compounds maintain the hexagonal layered structure.

Electrical conductivities for the sintered pellets of $Li_{1.075}V_{0.925-x}M_xO_2$ (M = Cr or Fe, x = 0, 0.01, 0.015, 0.02, 0.025) were measured by van der Pauw method. As shown in Fig. 3. $Li_{1.075}V_{0.925-x}Fe_xO_2$ samples exhibit higher electrical conductivities than $Li_{1.075}V_{0.925-x}Cr_xO_2$. The previous result suggests that the mixed valency as well as the enhanced interaction between the metal ions in the contracted edge-shared MO_6 octahedra in $Li_{1.075}V_{0.925}O_2$ lead to an increased electrical conductivity [9]. Although M–O distance increases with doping, the highest electrical conductivity is achieved in $Li_{1.075}V_{0.9}Fe_{0.025}O_2$. This could be due to the mixed valency and the larger particle size, as well as the lower strain in $Li_{1.075}V_{0.925-x}Fe_xO_2$ structure as Fe^{3+} ion has a similar radius with V^{3+} ion.

The results of charge and discharge of various $Li_{1.075}V_{0.925-x}M_xO_2$ (M = Cr or Fe, $0 \le x \le 0.025$) samples are shown in Fig. 6. $Li_{1.075}V_{0.9}Fe_{0.025}O_2$ exhibits the first charge capacity of 400 mAh g^{-1} at 0.1 C-rate. This value suggests 1.3 mol of lithium reacted with 1 mol $Li_{1.075}V_{0.9}Fe_{0.025}O_2$. $Li_{1.075}V_{0.9}Fe_{0.025}O_2$ exhibits

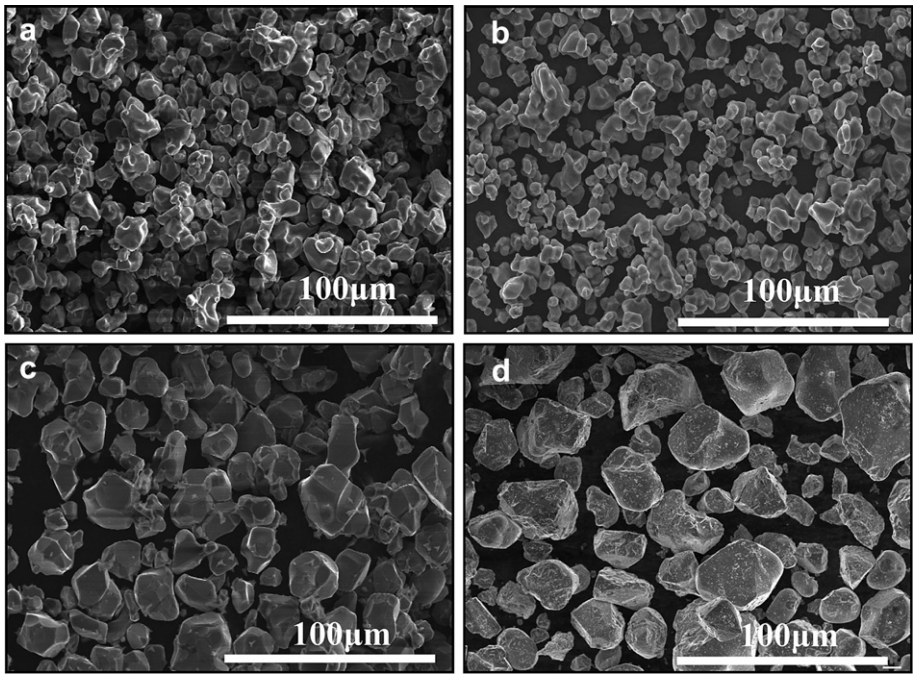

Fig. 4. S.E.M. pictures of various samples (a) $Li_{1.075}V_{0.91}Cr_{0.015}O_2$, (b) $Li_{1.075}V_{0.9}Cr_{0.025}O_2$, (c) $Li_{1.075}V_{0.91}Fe_{0.015}O_2$, and (d) $Li_{1.075}V_{0.9}Fe_{0.025}O_2$.

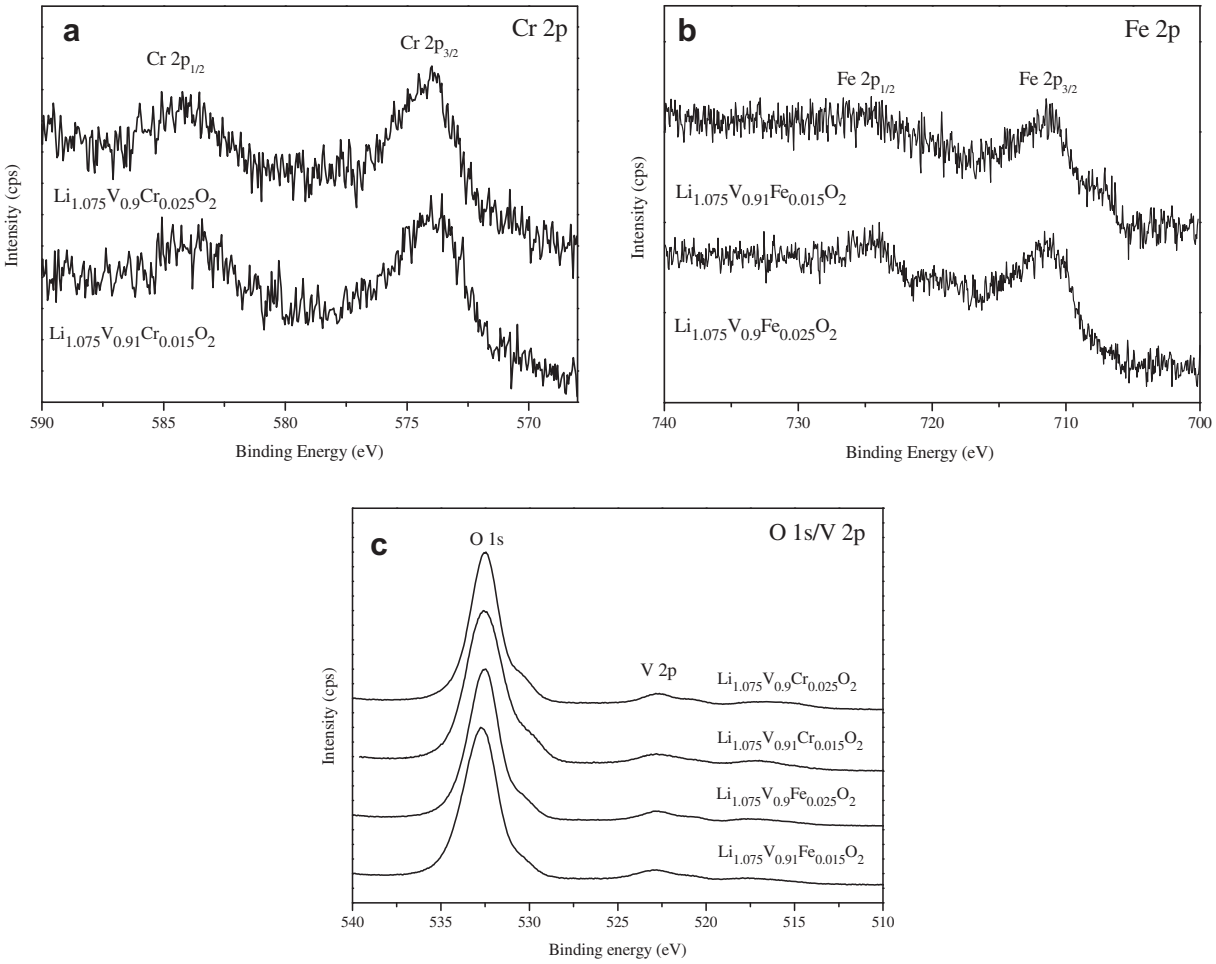

Fig. 5. XPS spectra of (a) Cr 2p, (b) Fe 2p and (c) O 1s and V 2p for the synthesized $Li_{1.075}V_{0.925-x}M_xO_2$ (M = Cr or Fe, $0 \le x \le 0.025$).

the first discharge capacity of 295 mAh g^{-1} at 0.1 C-rate and an excellent rate capability (235 mAh g^{-1} at 5 C-rate). Rate capability of cell is determined by the rate of reaction as well as the electronic transport. Lithiation reaction is recently explained by an insertion of lithium ion in the tetrahedral sites of $Li_{1+x}V_{1-x}O_2$ [10]. Compared to other compositions, a higher rate capability of $Li_{1.075}V_{0.9}Fe_{0.025}O_2$ might be due to its higher electrical conductivity. In addition to that, a higher electrode density can be achieved by large and strong particles of $Li_{1.075}V_{0.9}Fe_{0.025}O_2$, and the electrical conduction is facilitated in the electrode of the cell. It has been reported that

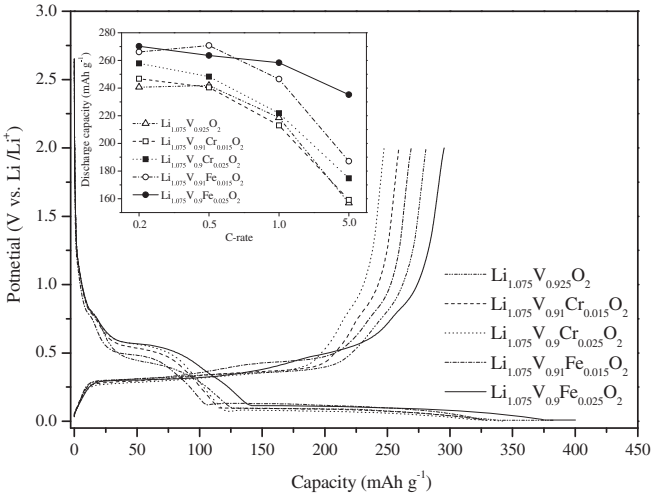

Fig. 6. Charge and discharge profiles of $Li_{1.075}V_{0.925-x}M_xO_2$ ($0 \le x \le 0.025$, M = Cr or Fe) with 0.1 C-rate charge/0.1 C-rate discharge, and inset shows the discharge capacities with various C-rates (0.2 C-rate charge/0.2, 0.5, 1, 5 C-rate discharge).

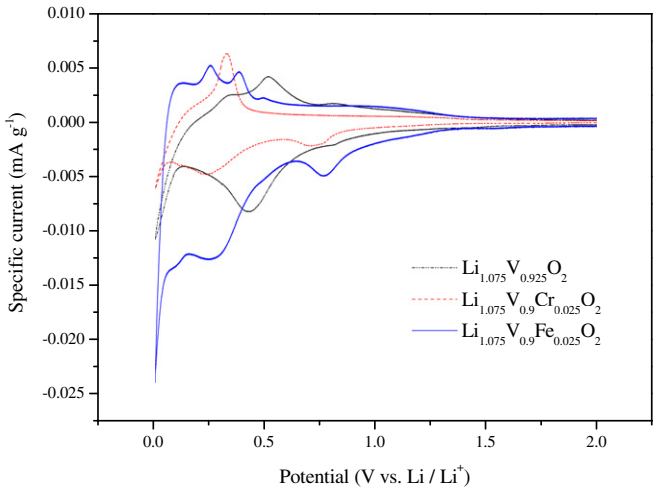

Fig. 7. Cyclic voltammograms of the first cycle.

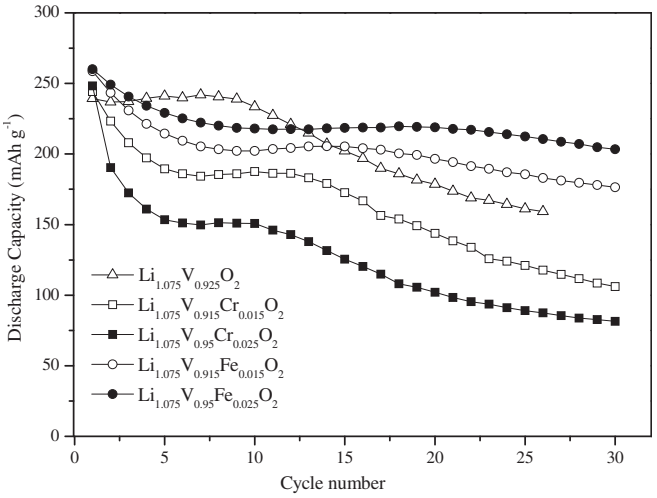

Fig. 8. Cyclabilities of $Li_{1.075}V_{0.925-x}M_xO_2$ ($0 \le x \le 0.025$, M = Cr or Fe).

a plateau at 0.4 V in the first charge curve of $Li_{1.1}V_{0.9}O_2$ disappears during the second charge [7], and this corresponds to the behavior of the reduction peak at ~0.4 V in the cyclic voltammogram [9]. As shown in Fig. 7, the first reduction peaks (0.81–0.71 V) of $Li_{1.075}V_{0.925-x}M_xO_2$ ($x = 0$ or 0.025, M = Cr or Fe) are related with an electrolyte reduction [10]. These peaks correspond to the small inflections (0.8–0.75 V) in the charge curves in Fig. 6. The second reduction peaks (0.43–0.27 V) of $Li_{1.075}V_{0.925}O_2$, $Li_{1.075}V_{0.9}Cr_{0.025}O_2$, and $Li_{1.075}V_{0.9}Fe_{0.025}O_2$ in the Fig. 7 correspond to the first plateaus in Fig. 6, these are irreversible lithiation reaction and vanish after the first cycle. Cyclabilities of various samples are shown in Fig. 8. Compared to the undoped sample, while chromium-doped samples give inferior performances, iron-doped samples show improved cycle lives. To examine the relation between the capacity retention and composition, surface morphologies of various electrodes after 30 cycles were observed by S.E.M. As shown in Fig. 9, extensive cracks on the surface of particles are observed in undoped and chromium-doped samples. A mechanism for the lithiation reaction was proposed by recent research [10]. These cracks resulting from the repeated volume changes due to the lithiation are the reason for the capacity fading. Iron doped particles have relatively little damages on the surface. Therefore, the strength of particle plays an important role in the cyclabilility. The results of compression tests for the various sized particles are shown in Fig. 10. The average strength of iron-doped particles is higher than those of chromium-doped and undoped particles. Iron-doping could have a positive effect to enhance the strength of particles. The exact effect of doping in the compounds and doping of other ions will be the focus of our continuous research.

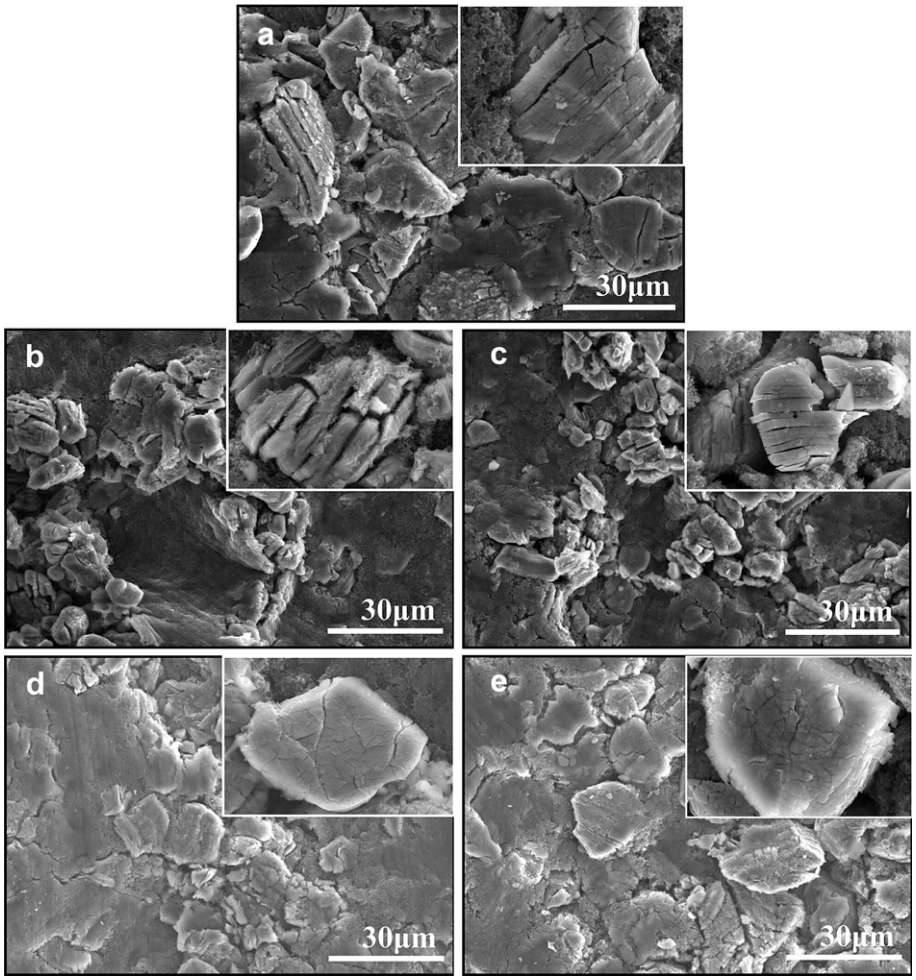

Fig. 9. S.E.M. images for the surface of various electrodes and particles after 30 cycles (a) $Li_{1.075}V_{0.925}O_2$, (b) $Li_{1.075}V_{0.91}Cr_{0.015}O_2$, (c) $Li_{1.075}V_{0.9}Cr_{0.025}O_2$, (d) $Li_{1.075}V_{0.91}Fe_{0.015}O_2$, and (e) $Li_{1.075}V_{0.9}Fe_{0.025}O_2$.

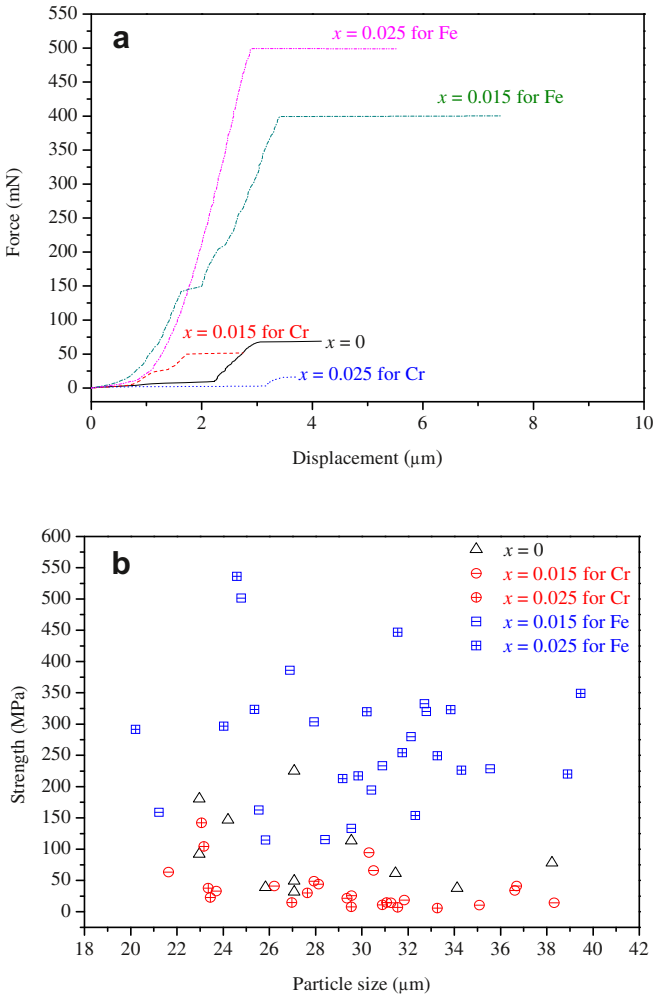

Fig. 10. Results of the compression tests for various $Li_{1.075}V_{0.925-x}M_xO_2$ (M = Cr or Fe, $0 \le x \le 0.025$) (a) plot of strength vs. displacement for the particle size of ~24 μm (b) plot of strength vs. particle size for various size particles.

4. Conclusions

$Li_{1.075}V_{0.925-x}M_xO_2$ (M = Cr or Fe, $0 \le x \le 0.025$) are successfully synthesized by solid-state reaction and the products give a single phase of the hexagonal layered structure with a space group of R-3m. The bond distances of Li–O, the angles of O_1–Li–O_4 and O_1–M–O_2 decrease and the bond distances of M–O, the angles of O_1–Li–O_2 and O_1–M–O_4 increase with the increased chromium- or iron-doping. The lattice constant of *a*-axis and MO_2-slab thickness increase and the lattice constant of *c*-axis and the inter-slab distance decrease with doping with chromium or iron. The electrical conductivity of $Li_{1.075}V_{0.925-x}Fe_xO_2$ is higher than $Li_{1.075}V_{0.925-x}Cr_xO_2$. XPS results suggest that the valence states of Cr and Fe in the sample are mainly +3 states. $Li_{1.075}V_{0.9}Fe_{0.025}O_2$ sample exhibits the highest discharge capacity among various samples investigated. $Li_{1.075}V_{0.9}Fe_{0.025}O_2$ also shows an excellent rate capability and capacity retention. Iron-doped particles have a higher strength than those of chromium-doped and undoped particles. Higher strength of iron-doped particle helps prevent the cracks during the lithiation reaction and enhance the cyclability of cells.

Acknowledgments

This work is supported by the Ministry of Knowledge Economy and KETEP (Korea Institute of Energy Technology Evaluation and Planning) for the development of materials and module of kWh-grade energy storage for the next generation.

References

[1] A. Mabuchi, K. Tokumitsu, H. Fujimoto, T. Kasuh, J. Electrochem. Soc. 40 (1995) 1041–1046.
[2] K. Nakahara, R. Nakajima, T. Matsushima, H. Majima, J. Power Sources 117 (2003) 131–136.
[3] P. Kubiak, A. Garcia, M. Womes, L. Aldon, J. Olivier-Fourcade, P.E. Lippens, J.C. Jumas, J. Power Sources 119-121 (2003) 626–630.
[4] C. Jiang, Y. Zhou, I. Honma, T. Kudo, H. Zhou, J. Power Sources 166 (2007) 514–516.
[5] K. Zaghib, M. Simoneau, M. Armand, M.J. Gauthier, J. Power Sources 81-82 (1999) 300–305.
[6] K.M. Colbow, J.R. Dahn, R.R. Haering, J. Power Sources 26 (1989) 397–402.
[7] N.S. Choi, J.S. Kim, R.Z. Yin, S.S. Kim, Mater. Chem. Phys. 116 (2009) 603–606.
[8] J.H. Song, H.J. Park, K.J. Kim, Y.N. Jo, J.S. Kim, Y.U. Jeong, Y.J. Kim, J. Power Sources 195 (2010) 6157–6161.
[9] W.T. Kim, Y.U. Jeong, H.C. Choi, Y.J. Kim, J.H. Song, H. Lee, Y.J. Lee, J. Appl. Electrochem. 41 (2011) 803–808.
[10] A.R. Armstrong, C. Lyness, P.M. Panchmatia, M.S. Islam, P.G. Bruce, Nat. Mater. 10 (2011) 223–228.
[11] M.M. Thackeray, L.A. Picciotto, W.I.F. David, P.G. Bruce, J.B. Goodenough, J. Solid State Chem. 67 (1987) 285–290.
[12] T. Yamashita, P. Hayes, Appl. Surf. Sci. 254 (2008) 2441–2449.
[13] J. Sainio, M. Aronniemi, O. Pakarinen, K. Kauraala, S. Airaksinen, O. Krause, J. Lahtinen, Appl. Surf. Sci. 252 (2005) 1076–1083.